Asariha et al, ***BioImpacts,*** 2020, 10(4), 217-226
doi: 10.34172/bi.2020.28
http://bi.tbzmed.ac.ir/

A new strategy for the green synthesis of chondroitin sulfate-reduced gold nanoparticles; *in vitro* evaluation of synthesized nanoparticles

Maryam Asariha[1,2], Azam Chahrdoli[2,3], Farshad Qalekhani[2], Mahnaz Ghowsi[2], Mehdi Fouladi[2], Maryam Gholamhosseinpour[2], Ali Fattahi[3]*

[1]Student Research Committee, School of Pharmacy, Kermanshah University of Medical Sciences, Kermanshah, Iran
[2]Pharmaceutical Sciences Research Center, Health Institute, Kermanshah University of Medical Sciences, Kermanshah, Iran
[3]Medical Biology Research Center, Health Technologies Institute, Kermanshah University of Medical Sciences, Kermanshah, Iran

Article Info

Article Type:
Original Article

Article History:
Received: 21 June 2019
Revised: 23 Nov. 2019
Accepted: 21 Dec. 2019
ePublished: 24 Mar. 2020

Keywords:
Chondroitin sulfate
Gold nanoparticles
In vitro evaluations
Green synthesis

Abstract

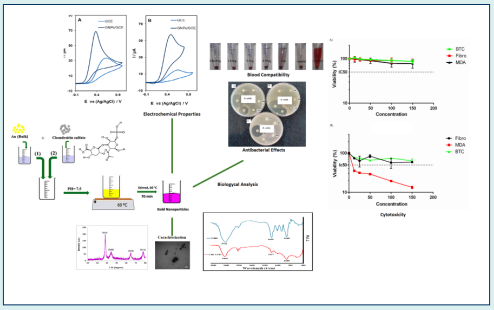

Introduction: The application of gold nanoparticles (GNPs) in medicine is expanding as an effective therapeutic and diagnostic compound. Different polysaccharides with high biocompatibility and hydrophilic properties have been used for synthesis and capping of GNPs. Chondroitin sulfate (CHS) as a polysaccharide possesses a wide range of biological functions e.g. anti-oxidant, anti-inflammation, anti-coagulation, anti-atherosclerosis, anti-thrombosis with insignificant immunogenicity and has not been used for the green synthesis of GNPs.

Methods: GNPs were synthesized using CHS, and their physicochemical properties were evaluated. The antibacterial activity of CHS-GNPs was estimated against both gram-positive and gram-negative bacteria. The cytotoxicity of CHS and CHS-GNPs was obtained by MTT (3-(4, 5-dimethylthiazol-2-yl)-2, 5-diphenyltetrazolium bromide) test, and the electrocatalytic activity of CHS-GNPs was investigated. The blood compatibility was evaluated by the *in vitro* hemolysis assay.

Results: The absorption band at 527 nm reveals the reduction of Au^{3+} into GNPs. The transmission electron microscopy (TEM) image displays the spherical shape of GNPs in the range of 5.8–31.4 nm. The CHS and CHS-GNPs at 300 µg/mL revealed a maximum DPPH (1, 1-diphenyl-2-picrylhydrazyl) scavenging activity of 73% and 65%, respectively. CHS-GNPs showed antibacterial activity against *Bacillus subtilis*, while CHS has no antibacterial activity. CHS-GNPs exhibited a cytotoxicity effect against MDA-MB-468 and βTC3 cancer cell lines, and the electrochemical study indicated a significant increase in electrocatalytic properties of CHS-GNPs coated electrode compared by the bare electrode. The hemolysis test proved the blood compatibility of CHS-GNPs.

Conclusion: The results indicate the advantages of using CHS to produce blood-compatible GNPs with antioxidant, cytotoxic, and electrochemical properties.

Introduction

In the present decade, the application of gold nanoparticles (GNPs) in medicine is expanding as effective therapeutic and diagnostic compounds; they have applied in photothermal therapy, drug delivery, gene delivery, mass spectroscopy, cell labeling, electrochemical biosensors and colorimetric detection of biological macromolecules e.g. nucleic acids, proteins, and glycosaminoglycans.[1-6] To synthesize GNPs, it is sufficient to use a factor that reduces the positive charged gold ions; various substances have been used to reduce gold ions and produce GNPs.[7] Among them, green synthesis of GNPs using natural compounds instead of harmful and toxic chemicals is preferred.[8,9]

Most recently, different polysaccharides with high biocompatibility, good bioactivity, and hydrophilic properties have been used for this purpose; they can

*Corresponding author: Ali Fattahi, Email: a.fatahi.a@gmail.com

synthesize and cap GNPs in one step.[10-13] In comparison with the green synthesis of GNPs by plant extracts, this method has the advantage of better control on the property of the nanoparticle shell. In herbal extract induced nanoparticles, the properties of the shell depend on the composition of the extract, which is by itself variable depending on the extraction method, used solvents, season, and area of plant harvesting. Among different polysaccharides, glycosaminoglycans (GAGs) have attracted huge attention because of their physiological function. While natural polysaccharides such as alginate and chitosan do not have any specific receptors, GAGs have unique receptors on human cells making them appropriate for the active targeting of nanoparticles. Because of their negative charge, they are appropriate for making a hydrogel using positively charged polymers and also for encapsulating of positively charged drugs by electrostatic interaction.[14-16]

Chondroitin sulfate (CHS), the most abundant GAGs of the human body, consists of a repeating disaccharide unit of glucuronic acid and N-acetyl-galactosamine, which are sulfated in variable positions. Its anti-angiogenic properties together with the over-expressing of its receptors in metastatic cancer cells make it an ideal candidate for cancer-targeted delivery system.[16-18] Furthermore, CHS possesses a wide range of biological functions e.g. anti-oxidant, anti-inflammation, anti-coagulation, anti-atherosclerosis, anti-thrombosis with insignificant immunogenicity. It also plays an important role in the regulation of cell morphogenesis, signal transduction, and the development of the central nervous system.[18,19] Although there is a report on using CHS coated GNPs as a theranostic compound for the diagnostic and treatment of cancer,[20] there are no reports on the synthesis and biological effects of one-step green synthesized GNPs. In this study, biocompatible GNPs were synthesized using CHS as a reducing and capping material. CHS-GNPs were characterized by UV-Vis spectroscopy, Fourier transform infrared (FT-IR), X-ray diffraction (XRD), transmission electron microscopy (TEM), and DLS analyses. Also, the antibacterial activity, the cytotoxicity, the antioxidant, and the electrochemical properties of CHS-GNPs were investigated.

Materials and Methods

Materials

Chloroauric acid ($HAuCl_4$), CHS, methanol, DMSO, MTT, DPPH, Mueller-Hinton agar (MHA), and broth were purchased from Sigma-Aldrich, USA. All other chemicals were analytical reagent grade and used without any further purification, purchased from Merck, Germany. Pancreatic beta-cell line (βTC3), MDA-MB-468, and all microorganisms including *Bacillus subtilis* (ATCC 6633), *Staphylococcus aureus (ATCC 25923), Staphylococcus epidermidis* (ATCC 12228), *Micrococcus luteus (PTCC 9341), Escherichia coli* (ATCC 25922) and *Salmonella enterica* (ATCC 9270) were purchased from Pasteur Institute Cell Bank, Tehran, Iran. Human fibroblast as the normal cell was isolated and purified by the procedure described in our previous work.[21] All the cell culture ingredients were supplied from Auto-cell Co., Poland.

Synthesis of chondroitin sulfate reduced gold nanoparticles (CHS-GNPs)

CHS-GNPs were produced in a stirring aqueous solution at the room temperature without using a UV light, autoclave, microwave, or laser irradiation under the following conditions; at first, 20 mL of $HAuCl_4$ (0.39 mg/mL in deionized water) with 10 mL of CHS (5mg/mL in deionized water) were mixed (at the volume ratio of 2:1), while pH of the solution was adjusted to 7.5. The solution obtained from the previous step was stirred at 60°C for 70 minutes when the ruby red color appeared. Then, the solution was centrifuged at 8000 rpm for 30 minutes, and prepared nanoparticles were washed properly three times. The synthesis procedure is illustrated in Scheme 1.

Characterization of CHS-GNPs

UV-Vis spectroscopy

UV-Vis spectrophotometric analysis, an indirect technique to detect the formation of nano-scale metal particles, was carried out by Analytik Jena, Specord 210 plus (Jena, Germany) at a resolution of 1 nm between 300-700 nm. The formation of CHS-GNPs was observed via the wavelength ranges of 500-550 nm.

Fourier transform infrared spectroscopy

CHS and CHS-GNPs were characterized by FT-IR to identify the functional groups by IR Prestige-21 Shimadzu Spectrometer, Kyoto, Japan. The FT-IR spectra were prepared in the spectral range of 400-4000 cm^{-1} at a resolution of 4 cm^{-1} and room temperature. Also, samples were pelleted using KBr powder.

XRD study

To confirm the crystalline nature of the synthesized CHS-GNPs, XRD was carried out on Xpertpro (Malvern Panalytical, Malvern, United Kingdom), which was operated at a voltage of 40 kV and a current of 30 mA with Cu K radiation.

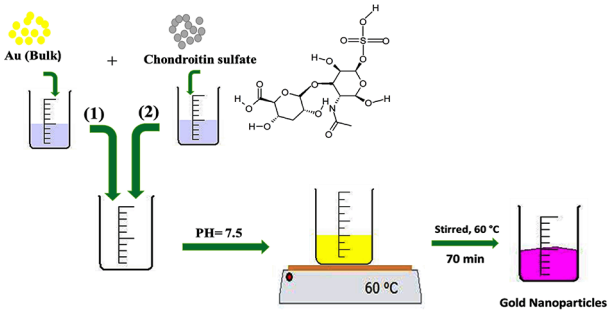

Scheme 1. The stepwise synthesized process of CHS-GNPs.

TEM analysis

TEM has been used to identify the morphology and particle size of CHS-GNPs using an LEO 906 microscope (Carl Zeiss, Oberkochen, Germany), with an accelerating voltage of 100 kV. Before analysis, GNPs were deposited on carbon-copper grids.

Dynamic light scattering and zeta potential

The particle size and surface charge (zeta potential) of CHS-GNPs were determined by the Nano ZS Zetasizer (Malvern Instruments Ltd., Malvern, United Kingdom) at a wavelength of 632.8 nm using He-Ne laser beam and the scattering angle of 173°. All particle sizes were measured at 25°C. The laser Doppler electrophoresis technique was performed to determine the zeta potential of CHS-GNPs in water.

DPPH free radical scavenging assay

The free radical scavenging ability of CHS and CHS-GNPs was predicted by DPPH assay using Chahardoli et al protocol with little modification. 0.1 mM solution of DPPH was prepared in methanol. 0.5 mL of different concentrations (50,100,150, 200, 250 and 300 µg/mL) of CHS and CHS-GNPs was mixed with 0.5 mL of DPPH solution, while mixtures were shaken well and incubated in the dark environment for 30 minutes. Finally, the absorbance of each mixture was recorded at 540 nm using the UV-Vis spectrophotometer. The mixer of 0.5 mL methanol and 0.5 mL DPPH solutions was recorded as a control.[22] By the following equation (1), the scavenging percentage of free radicals was determined:

$$\text{DPPH free radical scavenging (\%)} = [(OD_{control} - OD_{sample})/ OD_{control}] \times 100 \quad (1)$$

Evaluation of cytotoxicity by MTT assay

Cell culture conditions

The cells were grown in Dubblico modified Eagle's medium (DMEM) supplemented with 10% (V/V) heat-inactivated fetal bovine serum, penicillin G (100 U/mL) and streptomycin (100 mg/mL) at 37°C in 5% CO_2 humified incubator. The medium was changed 2-3 days and sub-cultured after 70%–80% cell confluency. Cells were cultured at a seeding density of 1.0×10^4 cells/well onto 96-well cell culture plate for the cell viability test.

Cell viability assay

Serial dilutions (1500, 1000, 500, 250, and 125 µg/mL) of CHS-GNPs and free-CHS were prepared in deionized water. About 20 µL of each solution was added at least to four wells of cell culture plates containing three different cells including βTC_3, MDA-MB-468, and human normal fibroblast at the final concentration of 10% for 48 hours. After this, the viability of cells was determined by the MTT assay. Briefly, 20 µL of MTT solution (5 mg/mL) was added to each well containing fresh medium and was incubated for 4 hours. Then, the medium was carefully substituted with 150 µL DMSO solution to solubilize the created purple formazan crystals in each well. Optical density was measured at 570 nm (reference wavelength of 630 nm) in a microplate reader (Synergy H1, BioTek, Winooski, USA). The absorbance of the untreated culture was set at 100% as control.

Antimicrobial activities by a disk-diffusion method

The disk-diffusion method was applied to define the antibacterial activity of CHS and CHS-GNPs on both gram-positive and gram-negative bacteria. The suspension of bacteria strains at final concentrations of 1.0×10^8 CFU/mL was swabbed on MHA plates by a sterile cotton swab. Then, sterile filter paper discs (about 6 mm in diameter) impregnated by the test compound at 4 different concentrations of 150, 300, 600, and 1200 µg/mL, were placed on the agar surface under aseptic condition. The plates were incubated for 24 hours at 37°C. As a positive control, 10 µg of gentamycin and 100 µg of piperacillin were used, while loaded on sterile filter paper discs. Finally, the inhibition zone of bacteria was measured using a Vernier caliper.

Electrochemical measurement procedure

Electrochemical measurements were performed using an Autolab PGSTAT101 potentiostat/galvanostat (Metrohm, Herisau, Switzerland) controlled by NOVA Auto-Lab software. An Ag/AgCl/KCl (3.0 M) as a reference electrode, a platinum wire as a counter electrode, and a glassy carbon electrode (GCE) or a modified GCE with CHS-GNPs as the working electrode in a conventional three-electrode cell were used, and all experiments were typically conducted at room temperature. The working electrode was prepared by a simple casting method. Before the modification of the electrode, the GCE was polished on a polishing cloth with alumina powder. A volume of 10 µL of the synthesized CHS-GNPs was cast directly on a GCE surface and the solvent was let evaporate at room temperature. The electrocatalytic activity of CHS-GNPs for 1.0 mM ascorbic acid (AA) and 1.0 mM dopamine (DA) oxidation was characterized by cyclic voltammetry (CV) in 0.1 M PBS (pH 7.4).[23]

In vitro hemolysis assay

The hemolytic effect of various concentrations of CHS-GNPs (62.5, 125, 250, 500, 1000 µg/mL) was evaluated and compared to the hemolytic effect of double distilled water and phosphate-buffered saline (PBS) as positive (100% hemolysis) and negative (0% hemolysis) controls, respectively. This test was performed using human fresh blood from female volunteers (25-30 years- old) according to the coming protocol: the blood was collected in tubes containing EDTA as anticoagulant and centrifuged at 800 ×g for 10 minutes to remove the plasma. The erythrocytes were washed three times with normal saline and 10 % suspension was prepared by using normal saline. The red

blood cell suspension was treated with each concentration of CHS-GNPs, double distilled water, or PBS, for 1 hour at 37°C temperature. Then, the samples were centrifuged at 13 400 rpm for 5 minutes, and 100 µL of supernatants was added to a well of 96-well plate and absorbance (Optical Density) was measured at 540 nm using a microplate reader, Synergy H1, BioTek.[24,25] Hemolytic percent was calculated as follows:

$$\text{Hemolysis \%} = (OD_{samples} - OD_{negative\ control}) / (OD_{positive\ control} - OD_{negative\ control}) \times 100 \quad (2)$$

Statistical analysis

Each experiment was completed at least three times. All the values were expressed as mean ± SEM. Statistical comparison among different groups was performed using one-way analysis of variance (ANOVA) and Tukey's test to determine the significant differences between groups at the level of $P < 0.05$. Statistical analyses were performed by SPSS (16) software.

Results

Characterization of CHS-GNPs

UV–Vis absorption spectra of CHS-GNPs at different time intervals have been displayed in Fig. 1. The characteristic surface plasmon resonance peak at about 527 nm, which was obtained at various reaction times, was an affirmation of CHS-GNPs synthesis. The intensity of the absorbance band was increased at intervals of 10 to 70 minutes, indicating that the concentration of CHS-GNPs was increasing, while the ruby red color was appearing.

The FT-IR spectra of CHS and CHS-GNPs were shown in Fig. 2. The FT-IR spectrum of CHS (Fig. 2A) indicated sharp bands at 3421, 2924, 1651, 1566, 1419, 1242, 1190, 1064, 1033, 590 cm^{-1}. The peak at 2924 cm^{-1} corresponded to CH_2 and CH_3 asymmetric stretching vibration aliphatic. The broad peak at 3650-2600 cm^{-1} was a feature of hydroxyl groups (OH) stretching vibration, and the peaks at 1190 and 1064 cm^{-1} were related to the C-O stretching vibration of OH. The peak at 1566 cm^{-1} corresponded to the bending vibration of the secondary amine of CHS, respectively. The peaks at 1242 cm^{-1} corresponded to N-C stretching vibration. The peak at 1651 cm^{-1} corresponded to -C=O (the carboxylic acid carbonyl stretching vibration). The FT-IR spectrum of CHS-GNPs (Fig. 2B) showed sharp bands at 3429, 2924, 2858, 1694, 1627, 1045, and 671 cm^{-1} approving that GNPs were coated by CHS.

Fig. 3 showed the XRD pattern of the synthesized CHS-GNPs which are four fine definite characteristic peaks within the 2θ range (10–80°). (111°), (200°), (220°), and (311°) crystalline planes belonged to the diffraction peaks of CHS-GNPs at 37.8°, 44.6°, 64.6°, and 77.5°, respectively. According to the pattern, CHS-GNPs consisted of a crystalline structure with a center cubic structure. Because of the high purity of CHS-GNPs, no additional peak was found in the XRD pattern.

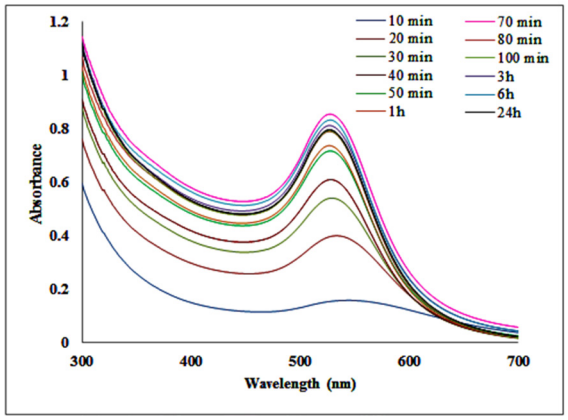

Fig. 1. The UV–Vis spectra of CHS-GNPs.

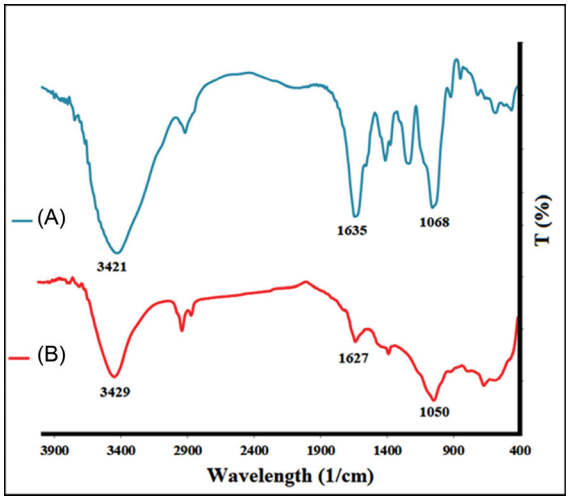

Fig. 2. The FT-IR spectrum of CHS (A) and CHS-GNPs (B).

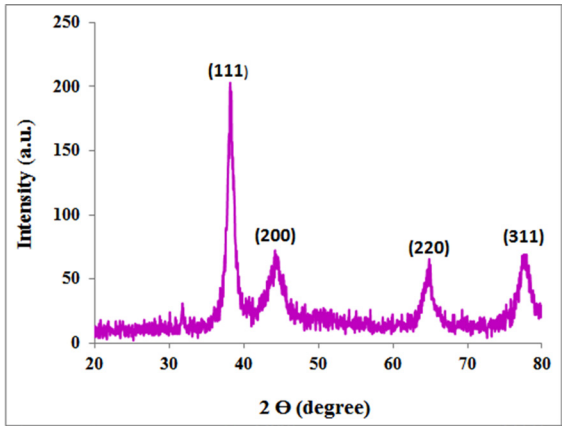

Fig. 3. The XRD spectrum of CHS-GNPs.

The TEM result gave a perfect detection of the size and shape of CHS-GNPs. As can be observed from Fig. 4, CHS-GNPs had mostly spherical shape morphology with the narrow particle size distribution in the range of 5.8–31.4 nm (Fig. 4A). The results of the DLS analysis displayed

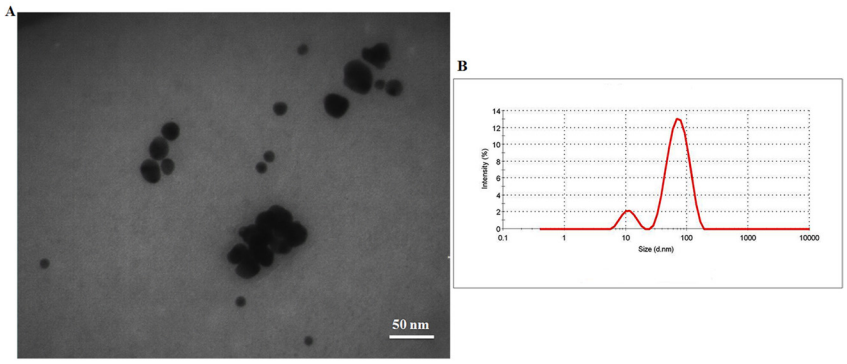

Fig. 4. (A) The TEM image and (B) DLS spectrum of CHS-NPS.

that the average hydrodynamic diameter of CHS-GNPs was 50.09 ± 2.52 nm (Fig. 4B) with the polydispersity index of 0.4.

The surface charge (stability) of CHS-GNPs was shown through the zeta potential. The zeta potential of CHS-GNPs was found to be -15.5 ± 5.09 mV, which confirmed the reasonable stability of CHS-GNPs.

Antioxidant properties

The free radical scavenging ability of CHS and CHS-GNPs was evaluated by DPPH assay, which showed the antioxidant properties of these compounds. As can be seen from Fig. 5, with increasing the concentrations (from 50 to 300 µg/mL), the DPPH scavenging activity of the CHS and CHS-GNPs increased. CHS and CHS-GNPs exhibited a maximum DPPH scavenging activity of 73 % and 65 % at the highest concentration (300 µg/mL), respectively.

Cytotoxicity

MDA-MB-468 and βTC3 cell lines together with human normal fibroblast cells were treated with both CHS-GNPs and free-CHS for 48 hours at final concentrations of 25, 50, 100 and 150 µg/mL. After the aforementioned treatment, the cytotoxicity effect was evaluated by the MTT assay. As shown in Fig. 6A, free CHS did not cause any cytotoxicity effect on all cell types. On the other hand, CHS-GNPs showed an anti-proliferation effect on MDA-MB-468 (IC50 > 100 µg/mL) and βTC3 (IC50 = 150 µg/mL) cell lines, while they have no cytotoxicity effect on human normal fibroblast (Fig. 6B).

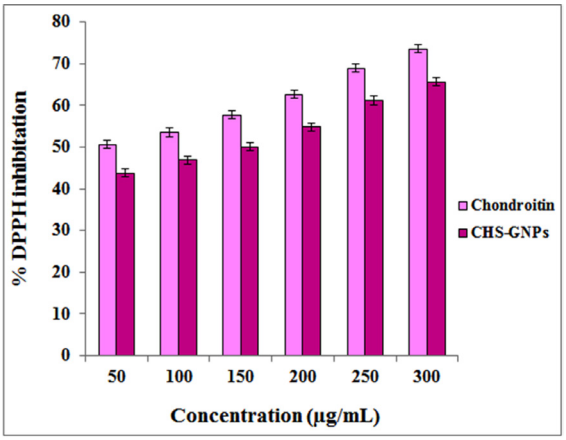

Fig. 5. The DPPH scavenging activity of CHS and CHS-GNPs at various concentrations.

Antimicrobial analysis

The disk diffusion assay was applied to determine the antibacterial activity of CHS and CHS-GNPs, where standard cultures of gram-positive and gram-negative bacteria were selected in this experiment. As shown in Table 1, CHS-GNPs exhibited antibacterial activity only

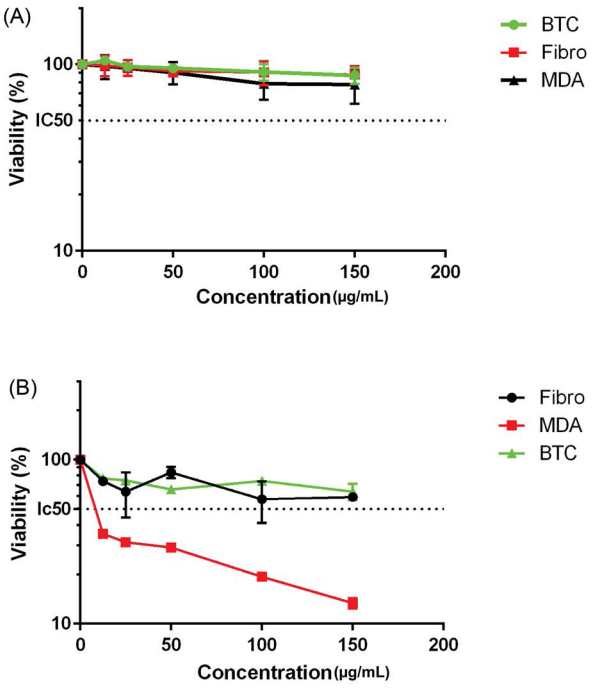

Fig. 6. *In vitro* cell viability of three various cell lines after treatment with different concentrations of (A) free-CHS and (B) CHS-GNPs. The cell viability is measured by MTT assay. The IC_{50} value was measured by plotting the percentage of proliferation values versus drug concentrations (µg/mL). About 40 µg of doxorubicin hydrochloride per well was used as a positive control. Data are expressed as the mean ± SEM of five separate experiments.

Table 1. Antimicrobial screening test of CHS and CHS-GNPs against bacterial strains

		Antimicrobial effects					
		Gram (+) bacteria				Gram (-) bacteria	
		B. subtilis	*S. aureus*	*S. epidermidis*	*M. luteus*	*E. coli*	*S. enterica*
Substance	CHS	-	-	-	-	-	-
	CHS-GNPs	+	-	-	-	-	-
Standard drug (control antibiotic)	Gentamycin	+	+	+	+	+	+
	Piperacillin	+	+	+	+	+	+

against *B. subtilis* (gram-positive bacteria), while CHS did not affect all bacteria at different concentrations. Effective concentrations of CHS-GNPs on *B. subtilis* were reported in Table 2 and also shown in Fig. 7. The inhibitory effect of CHS-GNPs started at 300 µg/mL with inhibition zones of 7.56 mm. As can be seen from Table 2, gentamycin and piperacillin as positive control were effective on all bacteria, which indicated the sensitivity of bacteria to treatment. Therefore, CHS-GNPs did not have efficient antibacterial properties, and even their activity against *B. subtilis* was weak compared to positive controls.

Electrocatalytic properties of CHS-GNPs

The electrocatalytic activity of CHS-GNPs for AA and DA oxidation was studied using CV in 0.1 M PBS (pH 7.4) with a scan rate of 100 mV/s. Fig. 8 shows the CVs of bare GCE and CHS-GCE modified with GNPs (CHS-GNPs-GCE) in the presence of 1.0 mM AA and 1.0 mM DA with the applied potential range from −0.1 to 1.0 V. The catalytic effect of GNPs can be observed by comparing CV curve of AA and DA at a surface of bare GCE and GCE modified with CHS-GNPs. Based on the obtained results, the peak potential for AA and DA oxidation at the bare electrode are about 605 and 645 mV, while the corresponding peak potentials at CHS-GNPs-GCE are 390 and 500 mV, respectively. Also, the presence of GNPs at a surface of GCE improved the oxidation peak currents of AA and DA about 2 and 3.9 times, respectively.

Table 2. Inhibition zone of the CHS-GNPs and positive controls against *B. subtilis* strains

	Concentration	Inhibition zones (mm)
CHS-GNPs	1200 µg/mL	11.36
	600 µg/mL	8.86
	300 µg/mL	7.56
	150 µg/mL	-
Gentamycin	10 µg	31.55
Piperacillin	100 µg	20.88

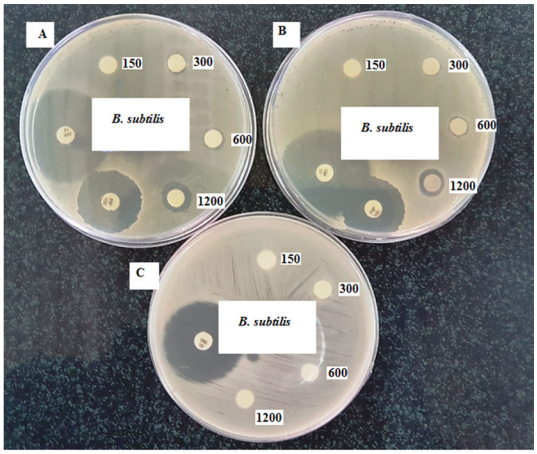

Fig. 7. The growth inhibition of *B. subtilis* after treatment with CHS-GNPs (A, B) and CHS (C) at different concentrations.

Hemolytic assay

In the present study, we evaluated the hemolytic potential of CHS-GNPs. The results of the *in vitro* hemolytic assay showed that different concentrations of CHS-GNPs (62.5, 125, 250, 500, 1000 µg/mL) had not significant hemolytic activity at 37°C (Fig. 9).

Discussion

As it is clear, UV-Vis spectroscopy is an important technique for approving the CHS-GNPs formation and provides information such as the crystal growth, size, and stability of nanoparticles. No significant increase and change in λ_{Max} were observed from 70 min to 24 hours (Fig. 1) demonstrating the colloidal stability of CHS-GNPs during the time.

Also, the XRD analysis is a powerful device for determining the purity and crystalline structure of the

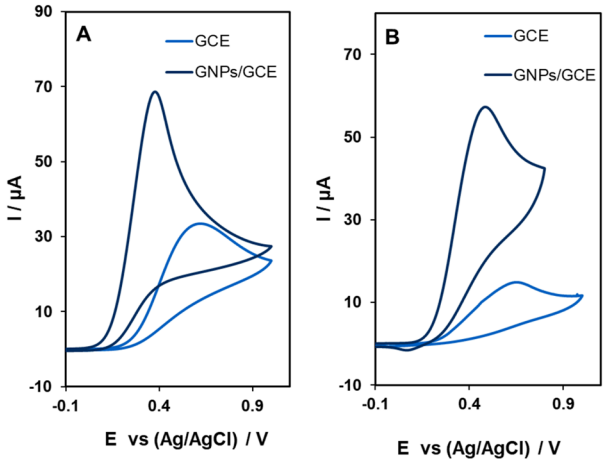

Fig. 8. The cyclic voltammograms of bare GCE and CHS-GNPs-GCE in 0.1M PBS (pH=7.4) containing 1.0 mM AA (A) and DA (B) at a scan rate of 100 mVs^{-1}.

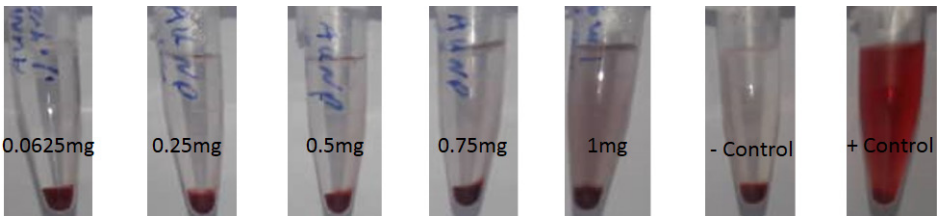

Fig. 9. The hemolysis test for red blood cells incubated with various concentration of CHS-GNPs (62.5, 125, 250, 500, and 1000 µg/ mL), double distilled water, and PBS for 1h. Double distilled water and PBS were used as positive (100% hemolysis) and negative (0% hemolysis) controls. Data are represented as the mean ± SE (n = 3).

synthesized nanoparticles. The average crystallite size of synthesized CHS-GNPs according to the Debye-Scherrer equation,[26] which reveals a relationship between XRD peak broadening and crystallite, was assessed around 14.94 nm. As shown in Fig. 4, the size of nanoparticles measured by the TEM method is different from that of DLS due to differences in their operating principles.[27] The particle size measured in the DLS method is larger because GNPs are coated by CHS, and the CHS shell swells in aqueous environments. The zeta potential of CHS-GNPs confirmed the logical stability of the CHS-GNPs. Due to the negative charges of CHS, the accumulation of CHS-GNPs was prevented by the repulsion of particles, which caused a stable colloidal solution.

The DPPH assay is a quick and accurate method for the evaluation of antioxidant effects. The DPPH scavenging activity of CHS was more than that of CHS-GNPs, which may be due to the configuration of sulfate groups in the CHS-GNPs. Previous studies approved the critical role of sulfate groups in antioxidant properties of CHSs; probably less accessible sulfate groups in CHS shell of GNPs caused their lower antioxidant activity.[28]

According to the cytotoxicity results, CHS-GNPs showed an anti-proliferation effect on MDA-MB-468 and βTC3 cell lines, while they have no cytotoxicity effect on human normal fibroblast. CHS-GNPs are selectively efficient on cancer cells and can potentially reduce the side effect of chemotherapy. The cellular uptake and translocation of GNPs across the cell membrane can be occurred by passive translocation and active endocytosis whereas GNPs smaller than 10 nm are probably taken up by the passive process, and the cellular uptake of larger nanoparticles can be occurred by receptor-mediated endocytosis.[29] Considering the size of the synthesized nanoparticles, it can be anticipated that receptor-mediated endocytosis it dominant way for uptake of CHS-GNPs.

Previously, it had been established that the cytotoxicity effect of materials in normal cells and cancer cells not similar where the receptors and the receptor expression on cancer and normal cells are different, and anti-proliferative pathways are diverse.[30] CHS as glycosaminoglycan, can bind to the cell-surface CD44 receptors and promote receptor-mediated endocytosis in cancer cells that specifically overexpress this receptor.[31] The overexpression of this established marker (CD44) for cancer stem cells (~4–5 folds) is responsible for metastasis and cancer progression.[32] MDA-MB-468 is a CD44 positive cell line, and previous studies indicated that the breast cancer cells overexpress the CD44 receptor,[33,4] and active targeting can be the reason for higher cytotoxicity of CHS-GNPs on MDA-MB-468. Besides, when CHS binds with CD44, it acts as a substrate for the P-selectins and leads to anti-metastatic properties. The anti-metastatic properties of sulfated glycans on breast and pulmonary cancers have already demonstrated.[32]

While our results indicated that CHS-GNPs showed the IC_{50} value of 100 and 150 µg/mL against MDA-MB-468 and βTC3 cell lines, Surapaneni et al showed that chemically synthesized citrate-capped GNPs (with a diameter of 25–30 nm and spherical shape) and cysteamine-capped GNPs (with a diameter of 35–40 nm and hexagonal shape) caused a significant decrease in the proliferation of MDA-MB-468 with an IC_{50} value of 384.35 and 313 µg/mL, respectively. They attributed the cytotoxicity effects of GNPs to the generation of oxidative stress in a dose-dependent manner in cancer cell lines; cysteamine-capped GNPs showed more oxidative stress in comparison to citrate-capped GNPs, while no oxidative stress was generated by GNPs in normal cells.[35]

Furthermore, the cytotoxicity of citrate-capped GNPs (20 nm) on the MRC-5 human fetal lung fibroblast cell line at different concentrations of studied by Li et al, where, they did not observe a significant difference in the percentage of cell death between the treatment and control groups after 24, 48, and 72 hours incubation, which confirms our founding on selective cytotoxicity of GNPs in cancer cells.[36]

Different mechanisms have been considered for GNPs' cytotoxicity; GNPs can induce diverse types of cell death through reactive oxygen species (ROS) production and mitochondrial function disturbance.[37] The generation of oxidative stress can be impairment in mitochondrial function as a consequence of elevated intracellular ROS. Further, GNPs cause cell cycle disruption, which is dependent on various factors including the physicochemical characteristics of the nanoparticle as well as the cell line.[38] The cytotoxicity depends on different factors including shape, size, surface functionality, charge, concentration, aggregation status, porosity, cell type, and experimental system variables, for example, temperature,

incubation period, and culture media. In addition to size and shape, surface chemistry may also play an important role in NP interaction with cells and subsequent cytotoxicity.[39]

Different parameters e.g. type of metal ions, size, and shape of nanoparticles can affect on antimicrobial activity of nanoparticles.[40,41] In the present study, CHS-GNPs exhibited antibacterial activity against *B. subtilis*, while CHS did not affect all bacteria at different concentrations. Since *B. subtilis* -the gram-positive bacteria- have a thick layer of peptidoglycan, the inhibitory effect of CHS-GNPs is probably due to their interaction with the bacterial cell wall proteins; thiol groups of proteins can interact with GNPs and cause adsorption of GNPs on the surface of the cell wall and destroy of cell wall's activities.[42]

The results of the electrochemical analysis indicated that the modification of electrode with CHS-GNPs had great improvement in the electrochemical response due to the excellent electrical property of CHS-GNPs.[43,44] Therefore, GHS-GNs are still electrochemically active, and GHS cap did not diminish the catalytic effect of GNPs.

The hemolysis is an *in vitro* assay to evaluate the blood compatibility of nanoparticles. Changes of red blood cells membrane integrity can be impaired by nanoparticles that in turn may result in hemolysis and maybe a serious threat to organism survival.[45] The hemocompatibility of CHS-GNPs in this study can be due to its size and negative zeta potential. According to Purohit et al results, the hemolysis percentage was increased by increasing the size (15-70 nm) and concentration (5-200 µg /mL) of synthesized GNPs with trisodium citrate; they reported 60% hemolysis in exposure to GNPs with 70 nm size at concentration 200 µg/mL.[46] Furthermore, GNPs biosynthesized by *Curcuma manga* indicated 10% of hemolysis at concentration 50 µg/mL.[47] Therefore, the blood compatibility of green synthesized CHS-GNPs can be an excellent and important property of them in biomedical applications.

Conclusion

The present results indicate that GNPs were synthesized with CHS as both reducing and stabilizing agent, whereas the procedure was simple and obtained by stirring and heating the mixture of $HAuCl_4$ and CHS aqueous solutions. The characterization of GNP by UV-Vis, FT-IR, XRD, TEM, and DLS analyses approved their synthesis. CHS-GNPs showed the antioxidant effect, but their effect was lower than that of CHS. CHS-GNPs revealed the cytotoxicity effects against MDA-MB-468 and βTC3 cancer cell lines without any significant effect on normal fibroblast cells. The antimicrobial property of CHS-GNPs was not significant, and the particles were just effective against *B. subtilis*. The electrochemical activity of AA and DA at CHS-GNPs-GCE indicated the electrocatalytic effect of the synthesized nanoparticles. Excellent blood compatibility of CHS-GNPs demonstrated by the hemolysis test. Altogether, our finding indicates CHS as a valuable reducing and capping agent for the synthesis of stable colloidal GNPs with antioxidant effect, blood compatibility, selective cytotoxicity on cancer cells, and efficient electrocatalytic effects.

Research Highlights

What is the current knowledge?

√ Different chemical and biological methods have been applied for the synthesis of gold nanoparticles.

√ The biological approach using plant extract and natural polysaccharides provide us versatile gold nanoparticle with different properties and biological activities.

√ Some gold nanoparticles showed hemolysis effect and blood incompatibility.

What is new here?

√ Synthesized CHS-GNPs using chondroitin sulfate as a reducing and capping agent showed antibacterial activity against *Bacillus subtilis*, selective cytotoxicity on MDA-MB-468 cell lines and valuable electrochemical properties.

√ Hemolysis test approved the blood-compatibility of CHS-GNPs.

Acknowledgments

The authors gratefully acknowledge the Research Council of Kermanshah University of Medical Sciences for financial support.

Funding sources

This study is part of an MSc thesis (ID: 97231) funded by Kermanshah University of Medical Sciences.

Ethical statement

This study was approved by the Research Ethics Committee at Kermanshah University of Medical Science (Code of Ethics: 3005792).

Competing interests

The authors declare no conflicting interests.

Authors' contribution

MA implemented the experiments and data handling. AC assisted in nanoparticle synthesis. FQ and MG performed blood tests. MF and MG contributed to some part of cytotoxicity tests. All the authors took part in writing and editing the manuscript. HN contributed in bacterial study, and AF was the supervisor of this work and edited the manuscript, prepared materials, designed experiments.

References

1. Ali MR, Wu Y, Ghosh D, Do BH, Chen K, Dawson MR, et al. Nuclear membrane-targeted gold nanoparticles inhibit cancer cell migration and invasion. Acs Nano 2017; 11: 3716-26. doi: 10.1021/acsnano.6b08345.
2. Chen Z, Luo S, Liu C, Cai Q. Simple and sensitive colorimetric detection of cysteine based on ssDNA-stabilized gold nanoparticles. *Anal Bioanal Chem* **2009**; 395: 489-94. doi:10.1007/s00216-009-2982-7.
3. Wang H, Huff TB, Zweifel DA, He W, Low PS, Wei A, *et al. In vitro* and *in vivo* two-photon luminescence imaging of single gold nanorods. *Proc Natl Acad Sci* **2005**; 102: 15752-6. doi:10.1073/pnas.0504892102.
4. Glazer ES, Zhu C, Massey KL, Thompson CS, Kaluarachchi WD,

Hamir AN, *et al.* Noninvasive radiofrequency field destruction of pancreatic adenocarcinoma xenografts treated with targeted gold nanoparticles. *Clin Cancer Res* **2010**; 16: 5712-21. doi: 10.1158/1078-0432.CCR-10-2055.
5. Wijaya A, Schaffer SB, Pallares IG, Hamad-Schifferli K. Selective release of multiple DNA oligonucleotides from gold nanorods. *ACS nano* **2008**; 3: 80-6. doi:10.1021/nn800702n.
6. Alexander CM, Hamner KL, Maye MM, Dabrowiak JC. Multifunctional DNA-gold nanoparticles for targeted doxorubicin delivery. *Bioconjug Chem* **2014**; 25: 1261-71. doi: 10.1021/bc500136r.
7. Nguyen DT, Kim D-J, Kim K-S. Controlled synthesis and biomolecular probe application of gold nanoparticles. *Micron* **2011**; 42: 207-27. doi: 10.1016/j.micron.2010.09.008.
8. Jin Y, Li Z, Hu L, Shi X, Guan W, Du Y. Synthesis of chitosan-stabilized gold nanoparticles by atmospheric plasma. *Carbohydr Polym* **2013**; 91: 152-6. doi: 10.1016/j.carbpol.2012.08.018.
9. Patra S, Mukherjee S, Barui AK, Ganguly A, Sreedhar B, Patra CR. Green synthesis, characterization of gold and silver nanoparticles and their potential application for cancer therapeutics. *Mater Sci Eng C* **2015**; 53: 298-309. doi:10.1016/j.msec.2015.04.048.
10. Li W, Li X, Su H, Zhao S, Li Y, Hu J. Facile synthesis of chondroitin sulfate-stabilized gold nanoparticles. *Mater Chem Phys* **2011**; 125: 518-21. doi: 10.1016/j.matchemphys.2010.10.023.
11. Tiwari AD, Mishra AK, Mishra SB, Arotiba OA, Mamba BB. Green synthesis and stabilization of gold nanoparticles in chemically modified chitosan matrices. *Int J Biol Macromol* **2011**; 48: 682-7. doi:10.1016/j.ijbiomac.2011.02.008.
12. Shao Y, Wu C, Wu T, Yuan C, Chen S, Ding T, *et al.* Green synthesis of sodium alginate-silver nanoparticles and their antibacterial activity. *Int J Biol Macromol* **2018**; 111: 1281-92. doi:10.1016/j.ijbiomac.2018.01.012.
13. Alam MS, Garg A, Pottoo FH, Saifullah MK, Tareq AI, Manzoor O, *et al.* Gum ghatti mediated, one pot green synthesis of optimized gold nanoparticles: investigation of process-variables impact using Box-Behnken based statistical design. *Int J Biol Macromol* **2017**; 104: 758-67. doi: 10.1016/j.ijbiomac.2017.05.129.
14. Köwitsch A, Zhou G, Groth T. Medical application of glycosaminoglycans: a review. *J Tissue Eng Regen Med* **2018**; 12: e23-e41. doi: 10.1002/term.2398.
15. Kemp MM, Kumar A, Clement D, Ajayan P, Mousa S, Linhardt RJ. Hyaluronan-and heparin-reduced silver nanoparticles with antimicrobial properties. *Nanomedicine* **2009**; 4: 421-9. doi: 10.2217/nnm.09.24.
16. Cheng K-m, Hung Y-w, Chen C-c, Liu C-c, Young J-j. Green synthesis of chondroitin sulfate-capped silver nanoparticles: Characterization and surface modification. *Carbohydr Polym* **2014**; 110: 195-202. doi: 10.1016/j.carbpol.2014.03.053.
17. Oommen OP, Duehrkop C, Nilsson B, Hilborn Jn, Varghese OP. Multifunctional hyaluronic acid and chondroitin sulfate nanoparticles: impact of glycosaminoglycan presentation on receptor mediated cellular uptake and immune activation. *ACS Appl Mater Interfaces* **2016**; 8: 20614-24. doi: 10.1021/acsami.6b06823.
18. Cho H-J, Oh J, Choo M-K, Ha J-I, Park Y, Maeng H-J. Chondroitin sulfate-capped gold nanoparticles for the oral delivery of insulin. *Int J Biol Macromol* **2014**; 63: 15-20. doi: 10.1016/j.ijbiomac.2013.10.026.
19. Zhao L, Liu M, Wang J, Zhai G. Chondroitin sulfate-based nanocarriers for drug/gene delivery. *Carbohydr Polym* **2015**; 133: 391-9. doi:10.1016/j.carbpol.2015.07.063.
20. Gurav D, Varghese OP, Hamad OA, Nilsson B, Hilborn J, Oommen OP. Chondroitin sulfate coated gold nanoparticles: a new strategy to resolve multidrug resistance and thromboinflammation. *Chem Commun* **2016**; 52: 966-9. doi:10.1039/C5CC09215A.
21. Safdari M, Shakiba E, Kiaie SH, Fattahi A. Preparation and characterization of Ceftazidime loaded electrospun silk fibroin/gelatin mat for wound dressing. *Fiber Polym* **2016**; 17: 744-50. doi:10.1007/s12221-016-5822-3.
22. Chahardoli A, Karimi N, Fattahi A, Salimikia I. Biological applications of phytosynthesized gold nanoparticles using leaf extract of *Dracocephalum kotschyi*. *J Biomed Mater Res A* **2019**; 107: 621-30. doi:10.1002/jbm.a.36578.
23. Khoshroo A, Hosseinzadeh L, Sobhani-Nasab A, Rahimi-Nasrabadi M, Ehrlich H. Development of electrochemical sensor for sensitive determination of oxazepam based on silver-platinum core–shell nanoparticles supported on graphene. *J Electroanal Chem* **2018**; 823: 61-6. doi:10.1016/j.jelechem.2018.05.030.
24. Devi LB, Das SK, Mandal AB. Impact of surface functionalization of AgNPs on binding and conformational change of hemoglobin (Hb) and hemolytic behavior. *J Phys Chem C* **2014**; 118: 29739-49. doi: 10.1021/jp5075048.
25. Choi J, Reipa V, Hitchins VM, Goering PL, Malinauskas RA.. Physicochemical characterization and in vitro hemolysis evaluation of silver nanoparticles. *Toxicol Sci* **2011**; 123(1): 133-43. doi: 10.1093/toxsci/kfr149.
26. Fornaguera C, Solans C. Methods for the *in vitro* characterization of nanomedicines—biological component interaction. *J Pers Med* **2017**; 7: 2. doi: 10.3390/jpm7010002.
27. Purohit R, Vallabani NS, Shukla RK, Kumar A, Singh S. Effect of gold nanoparticle size and surface coating on human red blood cells. *Bioinspir Biomim Nanobiomat* **2016**; 5: 121-31. doi:10.1680/jbibn.15.00018.
28. Foo Y, Periasamy V, Kiew L, Kumar G, Malek S. Curcuma mangga-mediated synthesis of gold nanoparticles: characterization, stability, cytotoxicity, and blood compatibility. *Nanomaterials* **2017**; 7: 123. doi: 10.3390/nano7060123.
29. Janic B, Liu F, Bobbitt KR, Brown SL, Chetty IJ. Cellular uptake and radio-sensitization effect of small gold nanoparticles in MCF-7 breast cancer cells. *J Nanomed Nanotechnol* **2018**; 9 :2. doi: 10.4172/2157-7439.1000499.
30. Shahani S, Hamzkanlu N, Zakeri N, Hosseinimehr SJ. Synergistic anti-tumoral effect of Achillea millefolium combined with bleomycin on prostate cancer cells. *Res Mol Med* **2015**; 3: 10-5. doi: 10.7508/rmm.2015.01.003.
31. Woude GF, Klein G, editors. Advances in cancer research. ed. F. V. W. George and K. George, Academic Press **2010**; 109, pp. 73–121.
32. Varghese OP, Liu J, Sundaram K, Hilborn J, Oommen OP. Chondroitin sulfate derived theranostic nanoparticles for targeted drug delivery. *Biomater Sci* **2016** ;4 :1310-3. doi: 10.1039/c6bm00335d.
33. Adavallan K, Krishnakumar N. Mulberry leaf extract mediated synthesis of gold nanoparticles and its anti-bacterial activity against human pathogens. *Adv Nat Sci* **2014**; 5: 025018. doi:10.1088/2043-6262/5/2/025018.
34. Campo G, Avenoso A, Campo S, Ferlazzo A, Calatroni A. Chondroitin sulphate: antioxidant properties and beneficial effects. *Mini Rev Med Chem* **2006**; 6: 1311-20. doi:10.2174/138955706778993012.
35. Surapaneni SK, Bashir S, Tikoo K. Gold nanoparticles-induced cytotoxicity in triple negative breast cancer involves different epigenetic alterations depending upon the surface charge. *Sci Rep* **2018**; 16: 12295. doi: 10.1038/s41598-018-30541-3.
36. Li JJ, Zou LI, Hartono D, Ong CN, Bay BH, Lanry Yung LY. Gold nanoparticles induce oxidative damage in lung fibroblasts in vitro. *Adv Mater* **2008**; 7: 138-42. doi. 10.1002/adma.200701853.
37. Sun H, Jia J, Jiang C, Zhai S. Gold nanoparticle-induced cell death and potential applications in nanomedicine. *Int J Mol Sci* **2018**; 19: 754. doi: 10.3390/ijms19030754.
38. Her S, Jaffray DA, Allen C. Gold nanoparticles for applications in cancer radiotherapy: Mechanisms and recent advancements. *Adv Drug Deliv Rev* **2017**;109: 84-101. doi: 10.1016/j.addr.2015.12.012.
39. Sasidharan A, Monteiro-Riviere NA. Biomedical applications of gold nanomaterials: opportunities and challenges. *Wiley Interdiscip Rev Nanomed Nanobiotechnol* **2015**; 7: 779-96. doi: 10.1002/wnan.1341.
40. Nadanaka S, Kinouchi H, Kitagawa H. Chondroitin sulfate–mediated N-cadherin/β-catenin signaling is associated with basal-

like breast cancer cell invasion. *J Biol Chem* **2018**; 293: 444-65. doi: 10.1074/jbc.M117.814509.
41. Yang C, He Y, Zhang H, Liu Y, Wang W, Du Y, *et al.* Selective killing of breast cancer cells expressing activated CD44 using CD44 ligand-coated nanoparticles *in vitro* and *in vivo*. *Oncotarget* **2015**; 6: 15283. doi: 10.18632/oncotarget.3681.
42. Tzircotis G, Thorne RF, Isacke CM. Chemotaxis towards hyaluronan is dependent on CD44 expression and modulated by cell type variation in CD44-hyaluronan binding. *J Cell Sci* **2005**; 118: 5119-28. doi:10.1242/jcs.02629.
43. Balakumaran M, Ramachandran R, Balashanmugam P, Mukeshkumar D, Kalaichelvan P. Mycosynthesis of silver and gold nanoparticles: optimization, characterization and antimicrobial activity against human pathogens. *Microbiol Res* **2016**; 182: 8-20. doi:10.1016/j.micres.2015.09.009.
44. Srivastava N, Mukhopadhyay M. Biosynthesis and characterization of gold nanoparticles using *Zooglea ramigera* and assessment of its antibacterial property. *J Cluster Sci* **2015**; 26: 675-92. doi:10.1007/s10876-014-0726-0.
45. Abdel-Raouf N, Al-Enazi NM, Ibraheem IB. Green biosynthesis of gold nanoparticles using G*alaxaura elongata* and characterization of their antibacterial activity. *Arab J Chem* **2017**; 10: S3029-S39. doi:10.1016/j.arabjc.2013.11.044.
46. Thirumalraj B, Rajkumar C, Chen S-M, Palanisamy S. One-pot green synthesis of graphene nanosheets encapsulated gold nanoparticles for sensitive and selective detection of dopamine. *Sci Rep* **2017**; 7: 41213. doi:10.1038/srep41213.
47. Mazloum-Ardakani M, Hosseinzadeh L, Khoshroo A. Ultrasensitive electrochemical immunosensor for detection of tumor necrosis factor-α based on functionalized MWCNT-Gold Nanoparticle/Ionic Liquid Nanocomposite. *Electroanalysis* **2015**; 27: 2518-26. doi:10.1002/elan.201500104.